An Automated Framework for Quantitative Porosity Assessment in CFRP Using Ultrasonic Attenuation and High-Resolution X-ray CT

M. Shayan Arani[1*], L. Laberge Lebel[1], R. Sicard[2], and A. Chahbaz[2], A. Saada[1]

[1] Advanced Composites and Fibers Structures Laboratory (ACFSlab), High Performance Polymer and Composite Systems (CREPEC), Polytechnique Montréal, Montreal, Canada

[2] TecScan Systems, St-Bruno-de-Montarville, Canada

* *Corresponding author (Morteza.shayan-arani@polymtl.ca)*

Keywords: *Aerospace; Porosity Measurement; Ultrasonic Attenuation; X-ray computed tomography; Carbon fiber reinforcement polymer*

1. Abstract

Porosity is a critical manufacturing defect in carbon fiber-reinforced polymer (CFRP) composite, as the presence of voids within the composite microstructure degrades mechanical performance and introduces variability that complicates qualification and quality assurance, particularly in aerospace applications. Ultrasonic attenuation has been widely investigated as a non-destructive indicator of porosity in composites; however, its sensitivity to pore morphology, size and spatial distribution associated with manufacturing-induced voids within the laminate remains an important challenge. This study builds upon prior work on ultrasonic attenuation-based porosity evaluation by incorporating high-resolution X-ray computed tomography (CT) measurements and enhanced automated data interpretation, enabling improved detection and quantification of small and low-contrast pores embedded within the composite material.

In this work, complementary automated ultrasonic inspections were performed on the same composite specimen to ensure spatial correspondence between ultrasonic and CT datasets. The attenuation-porosity relationship obtained from the original dataset. Combining higher-resolution CT data with matched ultrasonic scans further highlights the influence of pore size distribution on variations in ultrasonic attenuation observed at a given volumetric porosity level.

In parallel, the data processing and interpretation software for ultrasonic attenuation-based porosity evaluation was significantly refined to improved robustness, usability, and automation. The enhanced platform introduces advanced visualization, standardized data selection, strengthened statistical analysis, and streamlined reporting, with the objective of reducing operator dependency and improving repeatability when processing large UT/CT datasets. Overall, the combined use of higher-resolution CT data, confirmatory ultrasonic testing, and the proposed automated framework established a reliable and standardized non-destructive approach for porosity characterization in aerospace composite materials.

2. Introduction

The increasing use of Carbon fiber-reinforced polymer (CFRP) laminates in aerospace, automotive, marine, and civil engineering structures has made reliable non-destructive evaluation (NDE) essential for manufacturing quality control and in-service assessment [1]. The superior performance of CFRP composites is mainly related to their heterogeneous and anisotropic microstructure. Carbon fibers provide high stiffness and strength, while the polymer matrix transfers load between fibers, protects the reinforcement, and helps maintain the overall integrity of the laminate. However, this microstructural complexity also increases the sensitivity of CFRP laminates to manufacturing defects. Voids, resin-rich regions, fiber waviness, delamination, and incomplete consolidation can be introduced during fabrication [3]. Among these defects, porosity is especially important because it can reduce mechanical performance, increase material variability, and promote early damage [4]. This is particularly critical in aerospace applications, where even small changes in void content, morphology, or spatial distribution may affect structural performance, and standard practice commonly requires porosity levels below 2% [5]. Among different NDE techniques, ultrasonic testing (UT) is widely used for CFRP inspection because of its sensitivity to internal defects, its ability to inspect relatively thick components, and compatibility with automated scanning systems [6]. UT assesses material integrity by analyzing changes in wave propagation, including amplitude, time-of-flight, and attenuation. For porosity evaluation, ultrasonic attenuation is particularly important because voids scatter and absorb part of the propagating wave energy, reducing the received signal amplitude. However, attenuation-based porosity evaluation remains challenging because ultrasonic attenuation is influenced not only by the total void content, but also by pore size, morphology, spatial distribution, laminate architecture, anisotropy, and inspection conditions [7]. In addition, this approach requires a calibration of the attenuation trend as a function of porosity. As a result, reliable quantitative porosity estimation often requires the fabrication of proper reference samples with known porosity levels to establish an attenuation–porosity relationship, combined with a suitable external mean of measuring porosity levels accurately. This dependence on fabricated reference samples is a major limitation and highlights the need for a more reliable and scalable NDE approach for porosity evaluation without such calibration samples. This limitation has motivated efforts to better understand and model the attenuation–porosity relationship, beginning with Martin's theoretical work in 1976 [8]. He proposed a theoretical relationship between attenuation and void diameter by assuming spherical voids with uniform size and regular distribution. Hale and Ashton [9] later extended this approach to spherical and disc-shaped voids, while Nair [10] developed a model for long cylindrical voids with elliptical cross-sections and examined the attenuation, frequency, and porosity relationship. Although these models provided useful insight, their agreement with experiments was mainly limited to low porosity levels or low frequencies. This limited agreement was largely associated with their simplified representation of void morphology. Due to the computational limitations at the time, voids were often modeled using idealized geometries, uniform size distributions, and regular spatial arrangements. Later studies addressed this limitation by incorporating randomness into the void morphology, allowing variations in void size, shape, orientation, and spatial distribution to be considered [11, 12]. However, random void models still rely on statistically generated void morphologies, which may differ from the actual void structure in CFRP. To address this limitation, Ding et al. [7] developed a real morphology void model using an image-based model. Their results demonstrated a non-unique relationship between porosity and ultrasonic attenuation coefficient, where similar porosity levels could produce different attenuation values depending on void size, shape, orientation, and spatial distribution. Therefore, although ultrasonic attenuation is a valuable indicator of porosity, the non-unique attenuation–porosity relationship and the sensitivity of the results to void morphology highlight the need for a more consistent, repeatable, and automated framework for data processing and interpretation.

In previous work, a non-destructive experimental approach was presented to calibrate the ultrasonic attenuation response to porosity using a large dataset obtained from a micro-CT system [13]. Building on that work, the present study further develops the data processing platform by redeveloping the original Python-based tool into a more user-friendly JavaScript-based software environment. The updated platform improves data visualization, export of results, statistical analysis, and reporting, with the objective of reducing operator dependency and improving repeatability in ultrasonic attenuation-based porosity evaluation. In parallel, additional ultrasonic inspections and micro-CT scans were performed on the same composite samples using two micro-CT systems with different resolutions. This allows the influence of CT resolution on measured porosity levels to be examined and compared with microscopy-based observations. In the next stage of this study, numerical simulation will also be incorporated to further investigate the influence of void morphology on ultrasonic attenuation and to support a more reliable interpretation of the attenuation–porosity relationship.

3. Sample Fabrication

A series of carbon composite samples was prepared in an earlier phase of this study [13], with different levels of porosity being purposely induced from controlled fabrication process variations. The samples were produced using a high-performance aerospace grade composite (Cycom 5320-1 8HS carbon fiber prepreg). The samples layup is a quasi-isotropic stacking sequence [0/90/±45]s consisting of eight plies producing a cured thickness of approximately 3.1 mm per panel. Figure 1 schematically illustrates the manufacturing setup used to fabricate the CFRP plates. The carbon-fiber plies were stacked on the mold and covered with a release film, caul plate, breather layer, and vacuum bag. The vacuum bag was sealed using tacky tape, and the vacuum hose was used to remove trapped air and apply consolidation pressure during processing. This vacuum-bagging configuration promotes laminate compaction and allows fabrication conditions to be controlled in order to produce samples with different porosity levels. A total of ten composite plates (12” × 12”) were fabricated using the same stacking method, but with deliberate process variations to generate different porosity levels. Unlike standard prepreg manufacturing, no intermediate debulking was performed, meaning the eight plies were stacked without vacuum or compaction between layers. This approach promoted void formation by reducing inter-ply contact. Different vacuum levels were intentionally applied during processing of each plate. These variations affect laminate compaction and air removal between plies, thereby promoting different levels of void formation. As a result, the fabricated plates provide a range of porosity levels suitable for correlation with ultrasonic attenuation and CT measurements.

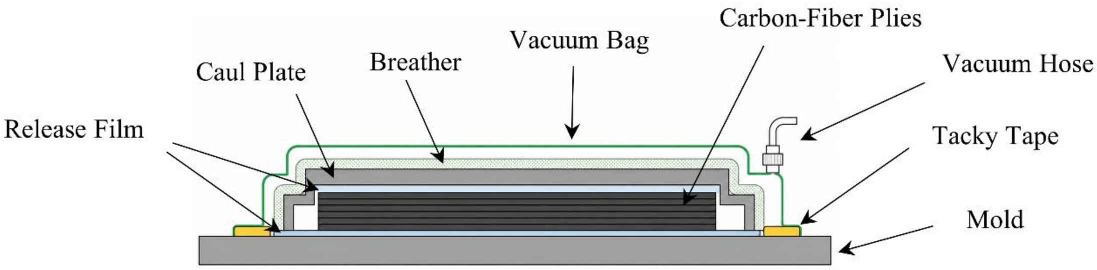

Figure 1. Method of manufacturing plates of carbon-fiber reinforced polymer (CFRP).

Each of the 12” x 12” carbon fiber plate was then subjected to ultrasonic inspection at TecScan using immersion C-Scan techniques. These scans provided uncalibrated attenuation maps that helped identify suspected areas presenting different levels of porosity. Smaller regions of interest of 100 mm x 26 mm were subsequently cut to build a set of reference samples for micro-CT scan analysis. Figure 3 shows an example of this selection process with the C-Scan image of the backwall amplitude echo acquired on Plate No. 2. In this image, light blue represents high echo amplitude (low porosity) while dark blue and green are associated with higher porosity content (lower backwall echo amplitude). The samples were selected to with various attenuation levels in order to obtain different porosity conditions. For example, the central region (Sample 2.1) presents high attenuation and is expected to contain higher porosity. In contrast, regions such as Samples 2.3 and 2.6 show lower attenuation levels and are expected to represent lower-porosity zones. This selection strategy led to samples with different porosity levels required for subsequent micro-CT characterization and comparison with ultrasonic attenuation data.

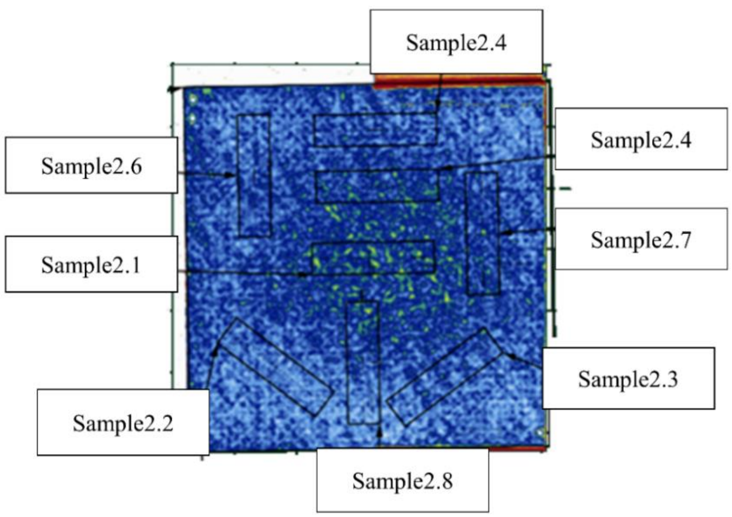

Figure 2. Example of an amplitude C-scan showing areas of interest for Plate No. 2.

4. Micro-CT Scan Investigation

The microtomography (CT-Scan) scanning is a frequently used solution to analyze composites porosity [14, 15]. The Figure 3 shows CT-Scan setup (Xradia 520 Versa, Zeiss) used in this goal. The Figure 3(a) present the setup with the x4 receptor used and the LE1 filter aligned with the X-Rays source. The Figure 3(b) show a global view of the 8.3 sample with the scan area encircled in blue and the Figure 3(c) do the same for the 2.1 sample. The CT-Scan is realized with a source set on 80kV and 7 W, and with a bin of 2. The field of view for the acquisition is centered on areas presented in the Figure 4, giving a voxel size of approximately 4 µm. A 400 takes acquisition (~20 min) is firstly run as a warmup for the machine and allowing a first pic at the file quality. Then the full 2400 takes acquisition is run (~160 min). The file is cleaned with a noise reduction filter step, removing the ambient noise in the file. The CT-Scan is finally analyzed using the software Dragonfly.

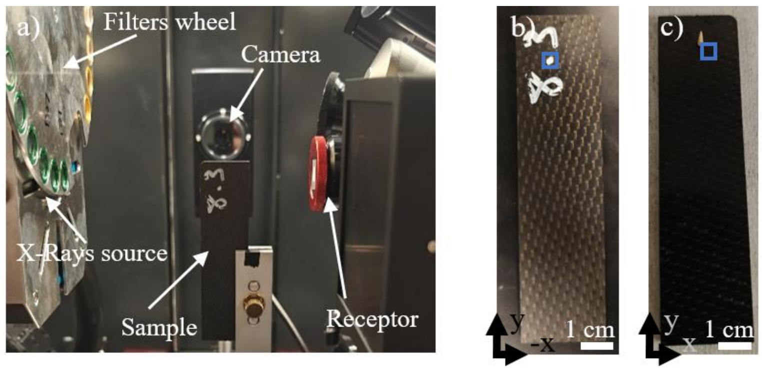

Figure 3. Illustration of the Xradia 520 Versa, Zeiss, Microtomography setup used in this study. In a), the setup detail, in b), a global view of the 8.3 sample with the microtomography view scope in blue and, in c), a global view of the 2.1 sample with the microtomography view scope in blue.

5. Ultrasonic Evaluation

The composite samples were scanned using a TS-3000 ultrasonic immersion scanner from TecScan Systems with the pulse-echo method. A flat, circular 5 MHz transducer with an element diameter of 6.35 mm (0.25 in), model V310-SU from Evident, was used for the measurements. Figure 4 shows the ultrasonic transducer positioned above the CFRP samples for pulse-echo scanning. Rubber spacers used to lift the samples from the bottom surface of the immersion tank are visible in these side views, their purpose being to prevent direct contact between the samples and the tank surface in the scanned areas. Since all samples had the same nominal thickness, the attenuation caused by voids was evaluated from the reduction in backwall echo amplitude expressed in dB referred to a common reference.

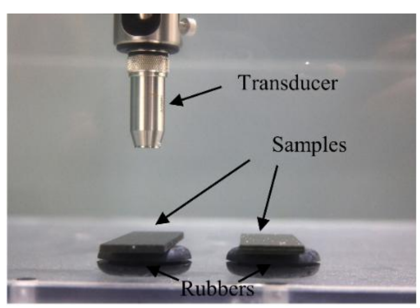

Figure 4. Ultrasonic immersion setup used for pulse-echo inspection, showing the transducer, CFRP samples, and rubber spacers used to lift the samples from the tank surface inside the immersion tank.

The samples were scanned at a resolution of 0.5 mm along both axes, making sure that the sample was located in the far field region of the probe and with the ultrasonic beam perpendicular to the entry surface. Figure 5 presents examples of C-scans of the backwall echo amplitude acquired from three different samples, along with the color scale representing the backwall amplitude. These samples show three different conditions. The high backwall echo amplitude, which is associated with low porosity content, appears in red in Figure 5(a). The low backwall echo amplitude, which is associated with high porosity content, appears in green in Figure 5(c). The orange region in Figure 5(c) represents an intermediate porosity condition between these two cases. It should be mentioned that the set of samples does not include a zero-porosity reference. However, all samples were scanned using the same probe excitation and wave reception settings in order to preserve the relative differences between samples and generate a relevant attenuation–porosity dataset.

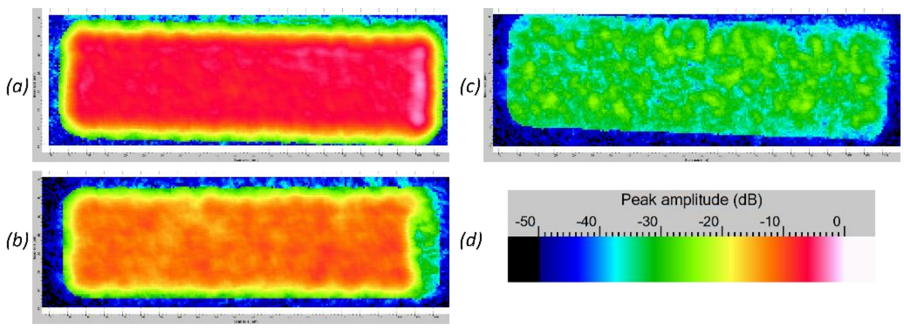

Figure 5. Examples of the backwall echo amplitude (dB) recorded on samples with expected (a) low, (b) medium and (c) high void contend; (d) The color scale indicates peak amplitude in dB.

6. Porosity Evaluation Software

A porosity evaluation software was previously developed to analyze the correlation between porosity volume and ultrasonic attenuation [13]. A new, more complete version of this software has recently been released, providing multiple analysis possibilities and calibration curves outputs. Figure 6 shows the flowchart of operations performed by the software. The objective and purpose of the software is to perform a spatial correlation between an ultrasonic C-Scan and CT-Scan data acquired on a set of samples, and to output local porosity volume percentage VS corresponding ultrasonic attenuation data points. Three analysis modes are currently proposed, as illustrated in figure 6 and described in the following sections: porosity % per attenuation C-Scan pixel (black dashed lines in figure 6), porosity % vs attenuation over the entire sample (red outline), and porosity % vs attenuation within small rectangular sections of the sample (white dashed lines).

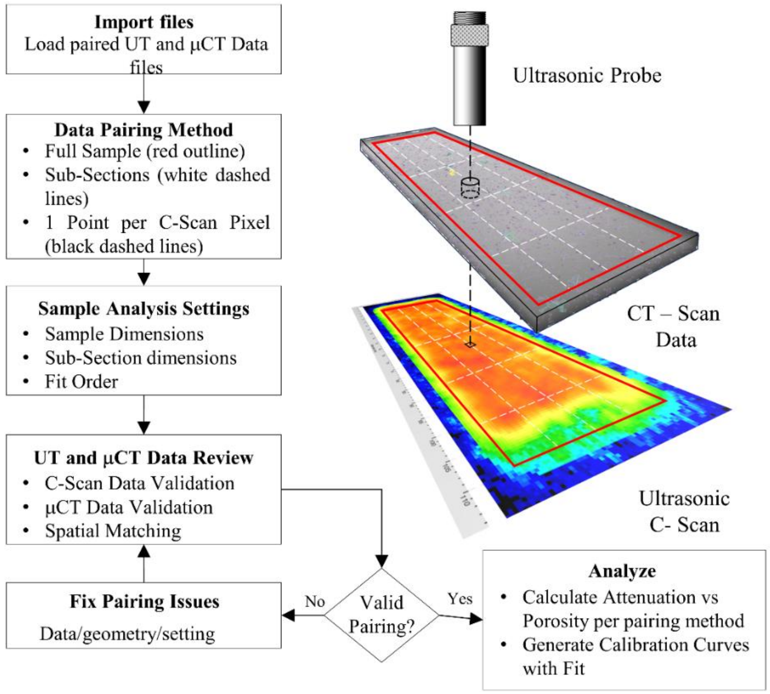

Figure 6. Operation flowchart of the porosity calibration and evaluation software, along with a schematization of the spatial correlation approaches described in sections 6.1 to 6.3.

6.1. Porosity % for the Entire Sample

The purpose of this mode is to reproduce calibration conditions found in the literature, where the average attenuation measured across an entire sample is shown to correlate with the overall volume porosity percentage of the sample [7, 15].

6.2. Porosity % per UT C-Scan Pixel

The objective of this option is to generate a large volume of attenuation vs porosity data points pair. Using the ultrasonic probe characteristics (element diameter and frequency), the ultrasonic scan type (immersion vs contact), and the scanning setup (pulse-echo vs transmission, probe-to-part distance), the ultrasonic beam diameter is first estimated at the position corresponding to the part surface. For a flat, circular transducer element of diameter D located at a distance X from the part surface greater than the near field, the beam diameter can be expressed as the width of the central lobe of the Airy pattern [16]:

$$BD = \frac{1.22\lambda X}{D} \tag{1}$$

While equation (1) is only true for a specific wavelength (λ), it provides a quantifiable order of magnitude of the beam diameter. Starting from this beam diameter, the volume porosity percentage provided by the CT-Scan data found in the cylindrical volume centered on each C-Scan image pixel is then calculated and paired with the pixel's ultrasonic attenuation value. This provides a highly localized measurement that is expected to be not only impacted by the volume porosity percentage, but by the pores morphology as well.

6.3. Porosity % for Sub-Sections of the Sample

The average ultrasonic attenuation measured across small rectangular surfaces is compared with the porosity content of the corresponding rectangular surface. This analysis mode is intended to estimate the porosity estimation error associated with the size of the selected sections in relationship with the calibration curve obtained by the previous method (entire sample). Figure 7 shows how CT-Scan is spatially correlated with C-Scan data, and how the analysis area is selected in the software.

Figure 7. Picture of the porosity evaluation software showing a spatial matching between CT-Scan data (red circles), ultrasonic C-Scan pixels position (blue dots), as well as the analysis area (semi-transparent green rectangle)

6.4. Additional Analysis

The original goal of the software is to provide multiple calibration options based on a regression of attenuation vs volume porosity percentage data sets. Although not shown in this paper, additional analysis tools were added to provide relevant calibration information such as a residue plot to estimate the porosity evaluation error using the calculated regression, as well as a standard deviation vs volume porosity percentage analysis.

7. Results

The new set of CT-Scan data was analyzed and compared with data that was previously acquired using a Nikon XT H 225 CT scanner with a voxel size of 20 µm. While this past study led to insightful conclusions, the CT-Scan estimation of the volume porosity was inconsistent with measurements made with a high resolution microscope, which systematically gave porosity counts by up to 10 times higher [13]. This inconsistency was attributed to the presence of small pores that were undetected due to the low-resolution CT-Scan. A comparative analysis of the volume porosity estimation was therefore performed with the new CT-Scan data, and compared with the ultrasonic attenuation C-Scan data. Samples labeled 2.1 and 8.3 were compared, while three additional samples were re-analyzed using the lower resolution CT-Scan data set to display the full tendency of the porosity vs attenuation graph of different analysis modes. Samples were segmented in 4 x 4 mm sections across the CT-Scan data set, excluding approximately 5 mm from the sides to avoid edge effects in the ultrasonic measurements. This provided multiple points per sample for the 20 μm voxel data set, and one porosity vs attenuation point for the new, 4 μm voxel CT-Scan data, which only probed a small section of the composite samples. A pixel-by-pixel analysis is also presented for the old data set for a beam diameter of 5.1 mm, as provided by equation (1). Figure 8 shows the plot of the volume porosity count as a function of ultrasonic attenuation obtained from both sets of CT-Scan data.

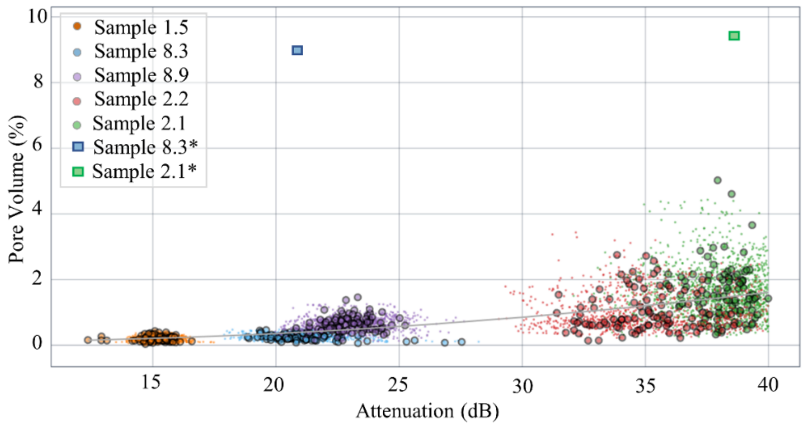

Figure 8. Comparison of the volumetric porosity percentage obtained by CT-Scan plotted as a function of ultrasonic attenuation. The asterisk (*) denotes new CT-Scan data set acquired with a voxel size of 4 mm. Outlined data points: analysis by section; dots: analysis per C-Scan pixel; line: second degree fit obtained from section analysis of the old data.

This plot supports the hypothesis that porosity count was previously under-evaluated, both samples showing a much higher volume porosity percentage with the new CT-Scan data. Since the analysis by sections produces data points that are spread around the regression, the same 4 × 4 mm square cut was analyzed with the old and new data for samples 2.1 and 8.3 to better illustrate the difference. The analysis of the same section resulted in a porosity count of 0.53% and 2.01% with the old CT-Scan data, and 9% and 9.36% with the new data for samples 8.3 and 2.1 respectively. It must also be noted that the pixel and section analysis modes, which are both sensitive to local pore morphology, resulted in a spread of data points that increases with the pore content. This is likely indicative of the presence of additional pore morphologies and sizes as the total pore volume increases, leading to different interactions between the ultrasonic waves and the pores; this is in phase with the conclusions of Ding et al. [7].

8. Conclusion

The measurement of the porosity content of composite samples using a high resolution CT-Scanner (4 μm voxel) resulted in a significant increase when compared to previous analysis of the same sample with lower resolution scan (20 μm). This highlights the need to use a proper device to set the porosity percentage baseline prior to the ultrasonic attenuation calibration. The various analysis modes of the porosity evaluation software presented in this paper offer valuable options to analyze the correlation between porosity and ultrasonic attenuation, as illustrated by the variations of ultrasonic attenuation observed for similar pore contents.

9. References

[1] X. Xu, G. Peng, B. Zhang, F. Shi, L. Gao, and J. Gao, "Material performance, manufacturing methods, and engineering applications in aviation of carbon fiber reinforced polymers: A comprehensie review," *Thin-Walled Structures*, vol. 209, p. 112899, Apr. 2025, doi: 10.1016/j.tws.2024.112899.

[2] D. S. Vijayan, A. Sivasuriyan, P. Devarajan, A. Stefańska, Ł. Wodzyński, and E. Koda, "Carbon Fibre-Reinforced Polymer (CFRP) Composites in Civil Engineering Application.

[3] K. Farnand, N. Zobeiry, A. Poursartip, and G. Fernlund, "Micro-level mechanisms of fiber waviness and wrinkling during hot drape forming of unidirectional prepreg composites," *Composites Part A: Applied Science and Manufacturing*.

[4] J. Shi, W. Wang, F. Liu, G. Xun, and P. Yang, "Effects of porosity on ultrasonic attenuation coefficient, shear properties and failure mechanisms of CF/EP laminates," *Heliyon*, vol. 10, no. 3, p. e25288, Feb. 2024.

[5] I. Tretiak and R. A. Smith, "A parametric study of segmentation thresholds for X-ray CT porosity characterisation in composite materials," *Composites Part A: Applied Science and Manufacturing*, vol. 123, pp. 10–24, Aug. 2019.

[6] TecScan Systems, A. Chahbaz, TecScan Systems, and R. Sicard, "Development of NDT Method for Porosity Evaluation in Composite Materials," *eJNDT*, vol. 30, no. 7, Jul. 2025, doi: 10.58286/31525.

[7] S. S. Ding, S. J. Jin, Z. B. Luo, J. Chen, and L. Lin, "Researches on the ultrasonic scattering attenuation of carbon fibre reinforced plastics with 2D real morphology void model," *Acoust. Phys.*, vol. 63, no. 4, pp. 490–495, Jul. 2017.

[8] B.G. Martin, "Ultrasonic attenuation due to voids in fibre-reinforced plastics," *NDT International*, vol. 9, no. 5, 1976.

[9] J. M. Hale and J. N. Ashton, "Ultrasonic attenuation in voided fibre-reinforced plastics," *NDT International*, vol. 21.

[10] S. M. Nair, D. K. Hsu, and J. H. Rose, "Ultrasonic Characterization of Cylindrical Porosity — A Model Study," in *Review of Progress in Quantitative Nondestructive Evaluation*, D. O. Thompson and D. E. Chimenti, Eds., Boston, MA: Springer US, 1987, pp. 1165–1174.

[11] L. Lin, X. Zhang, J. Chen, Y. Mu, and X. Li, "A novel random void model and its application in predicting void content of composites based on ultrasonic attenuation coefficient," *Appl. Phys. A*, vol. 103, no. 4, pp. 1153–1157.

[12] L. Lin, J. Chen, X. Zhang, and X. Li, "A novel 2-D random void model and its application in ultrasonically determined void content for composite materials," *NDT & E International*.

[13] A. Chahbaz and R. Sicard, "Development of NDT Method for Porosity Evaluation in Composite Materials," *eJNDT*, vol. 30.

[14] M. Mehdikhani, I. Straumit, L. Gorbatikh, and S. V. Lomov, "Detailed characterization of voids in multidirectional carbon fiber/epoxy composite laminates using X-ray micro-computed tomography," *Composites Part A: Applied Science and Manufacturing*.

[15] Y. Li, Y. Chi, S. Han, C. Zhao, and Y. Miao, "Pore-throat structure characterization of carbon fiber reinforced resin matrix composites: Employing Micro-CT and Avizo technique," *PLOS ONE*, vol. 16.

[16] Y. Ishii, S. Biwa, and A. Kuraishi, "Influence of porosity on ultrasonic wave velocity, attenuation and interlaminar interface echoes in composite laminates: Finite element simulations and measurements," *Composite Structures*.

[17] J. W. Goodman, *Introduction to Fourier Optics*, 3rd ed. Roberts & Company, 2005.